IEEE Photonics Journal
An IEEE Photonics Society Publication

Open Access

Anatomy of Phase Locking in Hyperparametric Oscillations Based on Kerr Nonlinearity

Volume 9, Number 3, June 2017

Hossein Taheri
Ali A. Eftekhar
Kurt Wiesenfeld
Ali Adibi

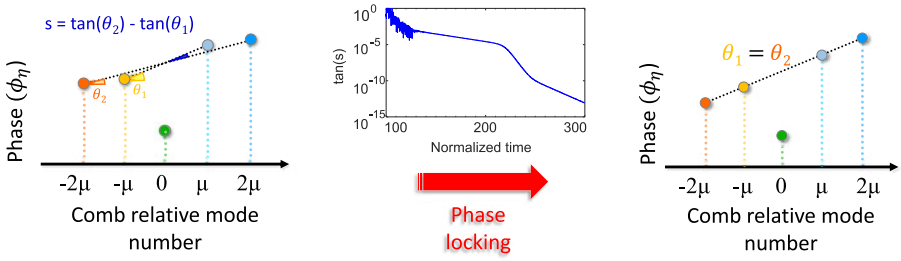

DOI: 10.1109/JPHOT.2017.2702647
1943-0655 © 2017 IEEE

Anatomy of Phase Locking in Hyperparametric Oscillations Based on Kerr Nonlinearity

Hossein Taheri,[1] Ali A. Eftekhar,[1] Kurt Wiesenfeld,[2] and Ali Adibi[1]

[1]School of Electrical and Computer Engineering, Georgia Institute of Technology, Atlanta, GA 30332 USA
[2]Center for Nonlinear Science, School of Physics, Georgia Institute of Technology, Atlanta, GA 30332 USA

DOI:10.1109/JPHOT.2017.2702647

Manuscript received February 20, 2017; revised April 29, 2017; accepted May 3, 2017. Date of current version May 24, 2017. This work was supported by the Air Force Office of Scientific Research under Grant FA9550-13-1-0032 (Dr. Gernot Pomrenke). Corresponding author: Hossein Taheri (e-mail: h.taheri@gatech.edu).

Abstract: We investigate the dynamical origin of synchronization and phase locking of hyperparametric oscillations in Kerr-nonlinear media. These oscillations occur in the presence of parametric gain and, although arising from modulational instability of random vacuum fluctuations with arbitrary phases, lead to phase-locked states in the form of pulse trains. Using few-mode approximations of the Lugiato–Lefever equation (LLE), we find that the pumped mode injection-locks to the driving laser pump following the Adler equation. Based on experimentally motivated assumptions, we derive analytical expressions, which reveal the essence of phase locking in frequency combs and confirm them through numerical integration of the LLE. Clear understanding of the phenomenon of phase locking in optical microresonators can lead to devising novel techniques for achieving phase-locked states or improving the coherence properties of frequency combs. Our results are mathematically generic and apply to other systems described by an externally driven damped nonlinear Schödinger equation.

Index Terms: Four-wave mixing, frequency combs, Kerr effect, mode-locked lasers, nanocavities.

1. Introduction

Phase-locked wideband optical frequency combs have in recent years been demonstrated in Kerr-nonliear media in multiple platforms [1]–[6]. These combs have shown to be ideally suited for ultra-high–capacity optical communication [7], [8] and pure radio-frequency (RF) wave generation [9]. The superior performance of micro-resonator-based combs for such applications hinges on the stable spacing between the comb teeth and their synchronized oscillations, which leads to the low phase noise of the generated comb teeth beat note. Phase locking of the frequency comb, i.e., the establishment of a temporally enduring relationship between the phases of the discrete frequencies comprising the comb, is key to the emergence of such stable comb lines.

Despite significant theoretical and experimental studies and demonstrations on “microcombs,” the phenomenon of phase locking in these nonlinear systems is not yet well understood. The generation of frequency combs in Kerr nonlienar media is described by a damped, externally driven

nonlinear Schrödinger equation (NLSE) [10], [11], which is also referred to as the Lugiato-Lefever equation (LLE) [12]–[15]. While it is known that this equation has sharply peaked solutions in the form of hyper-parametric oscillations (or Turing patterns) and solitons [4], [10], [11], [13], [14], [16], [17]—which evidence phase-locked states—the temporal evolution of the comb teeth phases toward these solutions has scarcely been studied. Clear understanding of the phenomenon of phase locking in optical microresonators can lead to devising novel techniques for achieving phase-locked states or improving the coherence properties of frequency combs, e.g., by seeding the comb generation process with pumps whose relative phases mimic the phase profile of a stable comb. It is also necessary for understanding and justifying some recent phase measurements of steady-state optical frequency combs [18], [19].

Matsko *et al.* found the steady-state offset of the pumped mode phase with respect to the rest of the combs in Turing patterns [20] and Loh *et al.* observed this offset experimentally [21], while Coillet and Chembo [22] provided an explanation of phase locking of optical microcombs in terms of the cascaded emergence of phase-locked triplets. Wen *et al.* [23] suggested a link between phase locking in parametric frequency combs and the famous Kuramoto model for the synchronization of globally-coupled nonlinear oscillators [24]. The analysis in [23] noted, through numerical simulations, that anti-symmetrization of the comb phase profile occurs prior to phase locking and soliton formation.

In this work, we report on a study of phase locking in Turing patterns based on 3- and 5-mode truncations of the LLE. The relative tractability of the truncated model allows us to find analytical expressions for the temporal evolution of the comb teeth phases, which clearly show how the frequency sidebands seeded by the random phase of vacuum fluctuations end up lying on a straight line. We show that the pumped mode of the comb is locked to the driving laser through the Adler equation and find that the anti-symmetrization of the sideband phases with respect to the pumped mode phase is predicted by the simplified 3-mode description. Considering the 5-mode truncation of the LLE, we are able to find an analytical expression describing how the phases of the comb teeth evolve, on a longer time scale, to their final locked state. It is noteworthy that the externally-driven, damped nonlinear Schrödinger equation has been used for describing a variety of physical phenomena in different nonlinear systems (see, e.g., [25] and references therein), and hence the results presented here apply to other NLSE systems as well.

2. Homogeneous Solutions of the Lugiato–Lefever Equation and Their Modulational Instability

The LLE is a nonlinear partial differential equation with periodic boundary conditions for the intra-cavity field envelope, in a slow and a fast time variable [13], [14], [26] or, equivalently, in time and the azimuthal angle around the whispering-gallery-mode resonator [15]. The non-dimensional form of the LLE reads

$$\frac{\partial \psi}{\partial \tau} = -(1 + \mathrm{i}\alpha)\psi - \mathrm{i}\frac{d_2}{2}\frac{\partial^2 \psi}{\partial \theta^2} + \mathrm{i}|\psi|^2\psi + F \tag{1}$$

where $\psi(\theta, \tau)$ and $F = F_{\mathrm{P}} \exp(\mathrm{i}\phi_{\mathrm{P}})$ are, respectively, the field envelope and pump complex amplitude, both normalized to the sideband generation threshold, α and d_2 are the pump-resonance detuning and second-order dispersion coefficient, each normalized to the half-linewidth of the pumped resonance, and τ is the time normalized to half of the photon lifetime in the resonator [15]. Depending on the pump power and detuning values, this equation may admit chaotic solutions [27], or solutions in the form of pulse trains called hyper-parametric oscillations (Turing rolls) as well as dissipative cavity solitons [4], [10], [11], [13], [14], [16], [17]. Turing rolls evolve from the CW flat solutions of the LLE through modulational instability (MI) [20], [28], whereas solitons can be generated through changing the pump power and frequency or through parametric seeding [29], [30]. Creation of sharply peaked pulses in this equation (rolls and solitons) relies on the establishment of a balance between nonlinearity, dispersion, gain, and loss [31]. Our aim is to understand how frequency side-bands generated from random vacuum fluctuations through the modulational instability of the spatially

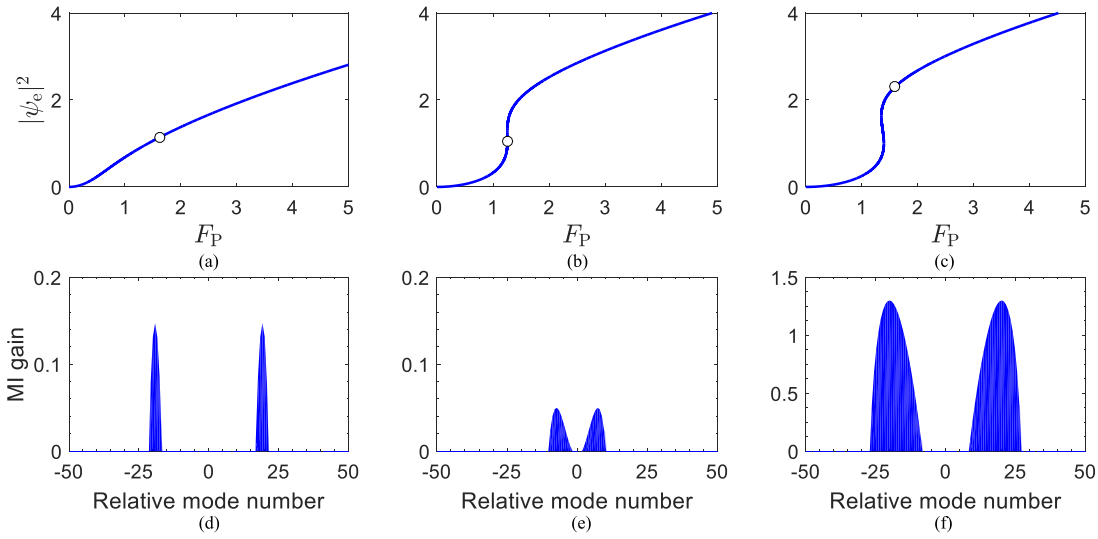

Fig. 1. (a)–(c) CW equilibrium $\rho_e = |\psi_e|^2$ solutions of the LLE vs. pump magnitude F_P and (d)–(f) modulational instability (MI) gain profile for different values of the detuning α. Each gain profiles in (d)–(f) corresponds to the point marked by the white dots on the $|\psi_e|^2$ versus F_P curve above it. Parameter values are (a) $\alpha = 0$, (b) $\alpha = 1.7607 = \sqrt{3.1}$, (c) $\alpha = 2.1$, (d) $(\rho_e, F_P) = (1.147, 1.63)$, (e) $(\rho_e, F_P) = (1.05, 1.257)$, and (f) $(\rho_e, F_P) = (2.25, 1.517)$. In all cases, $d_2 = -0.0124$. Note the difference between the y-axis scale in (f) and that in (d) and (e).

homogeneous solutions of the LLE phase lock to create sharply peaked pulses. Therefore, below we will briefly review bistability and MI gain for the LLE.

The simplest steady-state solutions of the LLE ($\partial/\partial\tau = 0$) is the spatially homogeneous or flat solution for which $\partial/\partial\theta = 0$ [4], [10], [32]–[34]. This CW equilibrium value ψ_e can be found from solving the cubic algebraic equation $\rho_e[1 + (\alpha - \rho_e)^2] = F_P^2$, where $\rho_e = |\psi_e|^2$. All solutions ρ_e of the latter equation for different values of F_P are non-negative. ρ_e vs. F_P is a function (single-valued) for $\alpha < \sqrt{3}$, but takes an S-shape and has three possible values for any value of F_P in a specific range of pump power when $\alpha > \sqrt{3}$. MI occurs in both of these regimes for ρ_e larger than the threshold $\rho_{Th} = 1$ (see Fig. 1). It can be shown [10], [34] that MI gain λ at the early evolution of the comb can be found from $\lambda = -1 + \sqrt{\rho_e^2 - (\alpha - d_2\eta^2/2 - 2\rho_e)^2}$, and will be positive if $\rho_e^2 - (\alpha - d_2\eta^2/2 - 2\rho_e)^2 \geq 1$. For the case of $\alpha > \sqrt{3}$ the middle negative-slope branch of the ρ_e vs. F_P curve is unconditionally unstable while the upper and lower branches demonstrate homogeneous bistability. Instability with respect to perturbations with non-zero relative mode numbers gives rise to Turing rolls on the upper branch as well as a small region on the lower branch for $\rho_e > 1$ and $\sqrt{3} < \alpha < 2$. Examples are shown in Fig. 1(b) and (c). Panels (d)–(f) in Fig. 1 show the MI gain profile for the points marked by the white dots on the $\psi_e - F_P$ plane in the upper panels (a)–(c), respectively. The Turing patterns corresponding to these MI gain profiles (detuning and pump power choices) are shown in Fig. 2.

It is worth noting that the Turing pattern in Fig. 2(a) is a so-called supercritical Turing pattern ($\alpha < 41/30$) while those in Fig. 2(b) and (c) are subcritical ($\alpha > 41/30$) [35]. While there are differences in existence threshold and shape between these LLE steady-state solutions [34], they are the same from the perspective of phase locking which is of interest to this work. We note that the spacing between the strongest sidebands of the pumped comb mode (upper row in Fig. 2(d)–(f)), or the peak of the MI gain profile (Fig. 1(d)–(f)) determines the number of peaks in the Turing patterns. The MI gain peak for Fig. 1(f) is on the 20th mode number, while the corresponding comb of Fig. 2(f) has 14 peaks. The reason is that the gain profiles in Fig. 1 shows the MI gain early on when the sidebands start to grow. If the gain profile is broad and falls on multiple mode numbers, apart from the mode number at the position of the MI gain maximum, nearby sidebands start occupying cavity modes as well, as is the case with Fig. 1(e) and (f). If the generated sharp peaks are too closely packed

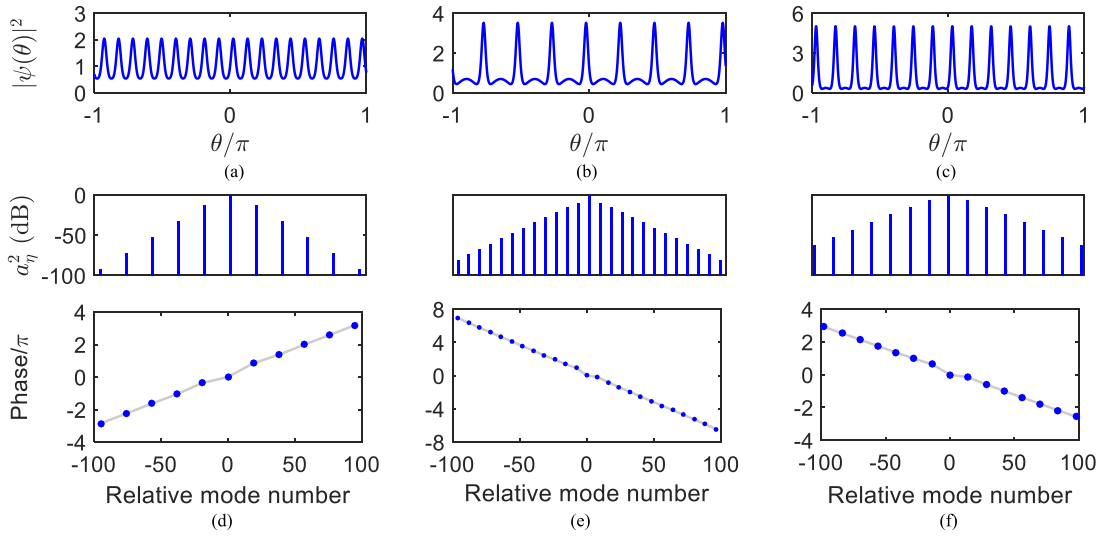

Fig. 2. Steady-state frequency combs for the parameters used for the gain profiles in Fig. 1(d)–(f). (a) and (d) correspond to Fig. 1(d), (b), and (e) to Fig. 1(e), and, finally, (c) and (f) to Fig. 1(f). (a)–(c) Intra-cavity field envelope. (d)–(f) Comb power spectra (top row) and phase spectra (bottom row). The phase spectra show the alignment of the phases for phase-locked combs.

together in the resonator, some of them may merge and the rest will readjust their positions on an equally-spaced grid [36]. The reduced number of Turing pattern peaks in the resonator corresponds to a reduction in the spacing between adjacent comb teeth and that is why in Fig. 2(f) the position of comb sidebands does not match the peak of MI gain profile in Fig. 1(f). While this was true for the Turing roll in the latter figure, the cascaded emergence of phase-locked comb teeth as a result of MI was the same as that of the simpler supercritical comb of Figs. 1(d) and 2(d). The integration of the LLE has been performed using the split-step Fourier transform method with random initial comb teeth phases and small random initial comb teeth powers to account for noise (random vacuum fluctuations).

3. Frequency-Domain Description of Optical Frequency Combs

Our goal is to explain how the sidebands which are seeded by noise (and hence have random phases) develop a simple phase relationship and give rise to sharply peaked pulses. Our approach is based on coupled nonlinear oscillators. The mathematical tool which allows us to go from the LLE to the coupled oscillator picture is the discrete-time Fourier transform (DTFT) or the Fourier series expansion. DTFT of (1), with the angle around the resonator θ and the comb mode number η as conjugate variables of the transform, leads to a set of coupled nonlinear ordinary differential equations (ODEs) [32]

$$\frac{\mathrm{d}\tilde{a}_\eta}{\mathrm{d}\tau} = -\left(1 + \mathrm{i}\alpha - \mathrm{i}\frac{d_2}{2}\eta^2\right)\tilde{a}_\eta + \mathrm{i}\sum_{l,\,m,\,n}\tilde{a}_l\tilde{a}_m^*\tilde{a}_n\,\delta_{\eta l m n \eta} + \tilde{F}_\eta \tag{2}$$

for the temporal evolution of the complex comb teeth amplitudes $\tilde{a}_\eta$ constituting the intra-cavity field envelope $\psi(\theta, \tau)$. For the Fourier pairs we have used the following equations and sign convention [37]:

$$\tilde{a}_\eta(\tau) = \frac{1}{2\pi}\int_{-\pi}^{\pi}\mathrm{d}\theta\,\psi(\theta, \tau)\,\exp(-\mathrm{i}\,\eta\theta) \tag{3}$$

and

$$\psi(\theta, \tau) = \sum_{\eta=-\infty}^{\infty} \tilde{a}_\eta(\tau) \exp(+\mathrm{i}\eta\theta). \tag{4}$$

The set of equations in (2) (for different integer values of the mode number η) is equivalent to the LLE. These equations are the same as the coupled-wave equations describing four-wave mixing and freqeuncy comb generation [32], [38]. In the coupled-modes picture, each comb mode labeled with the integer η is a nonlinear oscillator and one of the coupled ODEs follows the temporal evolution of its complex amplitude $\tilde{a}_\eta(\tau)$. In (2), δ_{ij} (for integers i and j) is the Kronecker delta, $\eta_{lmn} = l - m + n$, and l, m, and n are integers; the summation runs over mode numbers l, m, and n satisfying $l - m + n = \eta$, a condition enforced by phase matching. The modes are numbered relative to the mode closest to the pump (the pumped mode) for which $\eta = 0$. We consider CW pumping and therefore $\tilde{F}_\eta = \delta_{0\eta} F_\mathrm{P} \exp(\mathrm{i}\phi_\mathrm{P})$, F_P being the pump magnitude as defined following (1) and ϕ_P representing its phase. In the frequency domain, Turing rolls have power spectra which usually have multiple-FSR spacing between their adjacent teeth. In the model introduced here, $\eta \in \{0, \pm\mu, \pm 2\mu, \ldots, \pm N\mu\}$, where N is a positive integer and the integer $\mu \geq 1$ is the mode number at which MI gain peaks (as in Fig. 1(e)–(f)) and the primary combs are generated [33], [34], [39].

As a natural consequence of the resonator chromatic and geometric modal dispersion and as evidenced by experiments and numerical simulations, in stable non-homogeneous solutions of the LLE (or the equivalent coupled ODEs of Eq. (2)), the power of the comb teeth falls off with increasing relative mode nubmer. Additionally, the power in the pumped mode is usually much larger than the other modes (see, e.g., [8] and the examples shown in Fig. 2(d)–(f)); a condition which we refer to as the strong pumping regime. In this regime, equations of motion for the comb teeth magnitudes a_η and phases ϕ_η can readily be found by using $\tilde{a}_\eta = a_\eta \exp(\mathrm{i}\phi_\eta)$ in Eq. (2), dividing by $\exp(\mathrm{i}\phi_\eta)$, and separating the real and imaginary parts. The resulting equations read

$$\begin{aligned}\frac{\mathrm{d}}{\mathrm{d}\tau}\ln(a_\eta) = &-1 + \frac{a_{-\eta}}{a_\eta} a_0^2 \sin(\phi_\eta + \phi_{-\eta} - 2\phi_0) + \frac{F_\mathrm{P}}{a_\eta}\cos(\phi_\mathrm{P} - \phi_\eta)\delta_{0\eta} \\ &- \frac{a_0}{a_\eta}\sum_l a_l\{2a_{\eta+l}\sin(\phi_0 - \phi_l + \phi_{\eta+l} - \phi_\eta) + a_{\eta-l}\sin(\phi_l - \phi_0 + \phi_{\eta-l} - \phi_\eta)\},\end{aligned} \tag{5}$$

$$\begin{aligned}\frac{\mathrm{d}}{\mathrm{d}\tau}\phi_\eta = &\, 2a_0^2 - \alpha + \frac{1}{2}d_2\eta^2 + \frac{a_{-\eta}}{a_\eta}a_0^2\cos(2\phi_0 - \phi_\eta - \phi_{-\eta}) + \frac{F_\mathrm{P}}{a_\eta}\sin(\phi_\mathrm{P} - \phi_\eta)\delta_{0\eta} \\ &+ \frac{a_0}{a_\eta}\sum_l a_l\{2a_{\eta+l}\cos(\phi_0 - \phi_l + \phi_{\eta+l} - \phi_\eta) + a_{\eta-l}\cos(\phi_l - \phi_0 + \phi_{\eta-l} - \phi_\eta)\}.\end{aligned} \tag{6}$$

The summation index $l \neq 0$ in these equations runs over all relative mode numbers with appreciable power (i.e., above measurement noise level in experiments) for the comb studied. In the absence of third- and higher-order dispersion and when the frequency dependence of the loaded quality factor of the resonator is negligible [20], [40], the power spectrum of the generated Turing patterns is symmetric with respect to the pumped mode [3], [4], [34]; this condition can be seen to clearly hold in Fig. 2. Hence, we focus in this work on the phase evolution as comb teeth powers grow symmetrically with time, i.e., respecting $a_\eta(\tau) = a_{-\eta}(\tau)$. Therefore, while (5) is included for completeness, we will not need to refer to it in what follows. The phase equations, however, will be used in our analysis in the following sections. We emphasize that no symmetry assumptions have been made about the comb teeth phases.

Because we consider the experimentally-motivated regime of strong pumping, we can consider a truncation of the set of equations in (2) in our study of phase locking based on MI. Similar truncated models have been successfully used in studies of nonlinear wave mixing dynamics in fibers [41], [42] and microresonator-based frequency combs [43], [44]. In the following sections, we first study the pumped mode and then consider 3- and 5-mode truncations of (2).

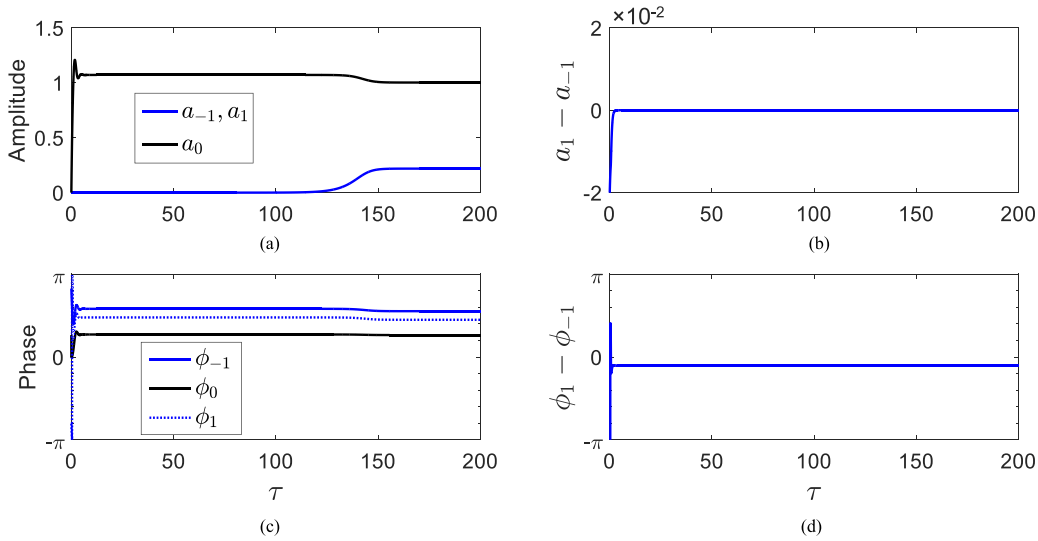

Fig. 3. Evolution of the comb teeth magnitudes and phases in the three-mode truncation of the LLE. (a) Pumped mode and sideband magnitudes. (b) Difference between the sideband magnitudes, which tends to zero soon after the comb starts evolving irrespective of the initial conditions, and confirming the power spectrum symmetry assumption. (c) Pumped mode and sideband phases. (d) Difference between the sideband phases, which tends to a constant, irrespective of the initial conditions. ± 1 refer to the first sideband pairs labeled $\pm\mu$ in the text.

4. Injection Locking of the Pumped Mode

We first consider the magnitude and phase equations for the pumped mode

$$\frac{\mathrm{d}}{\mathrm{d}\tau}\ln(a_0) = \frac{F_\mathrm{P}}{a_0}\cos(\phi_\mathrm{P} - \phi_0) - 1 \tag{7a}$$

$$\frac{\mathrm{d}\phi_0}{\mathrm{d}\tau} = \frac{F_\mathrm{P}}{a_0}\sin(\phi_\mathrm{P} - \phi_0) - \alpha + a_0^2. \tag{7b}$$

These pumped mode magnitude and phase equations include no linear contributions from $a_{\eta\neq 0}$ and, as a result, for the strong pumping regime we have dropped corrections arising from the primary and secondary sidebands (i.e., a_η^2 terms with $\eta = \pm\mu, \pm 2\mu$) in these equations. (We will verify the validity of this approximation using numerical integration of the truncated equations and the full LLE in what follows.) Hence, the pumped mode equations can be studied independently of the sidebands.

Numerical integration of the pumped mode equations shows that a_0 settles on a fast time scale to the equilibrium intra-cavity field $a_0 = |\psi_\mathrm{e}|$ [45]. After the sidebands $a_{\pm 1}$ start to grow (i.e., at $\tau \approx 130$ in Fig. 3(a) and (c)), the relative change in the pumped mode power is small. Subsequently, a_0 can be treated as a constant to first order in $a_{\eta\neq 0}$. With that in mind, the phase equation, (7b), can be written as

$$\frac{\mathrm{d}\Phi_0}{\mathrm{d}\tau} = -B(\sin\Phi_0 - K) \tag{8}$$

where $\Phi_0 = \phi_\mathrm{P} - \phi_0$, $B = F_\mathrm{P}/a_0$, and $K = a_0(\alpha - a_0^2)/F_\mathrm{P}$. This equation is exactly in the form of the Adler equation for injection locking [46]. In his 1946 paper, Adler showed that the condition for synchronization through injection locking is $|K| < 1$. This condition corresponds to

$$|\alpha - a_0^2| < \frac{F_\mathrm{P}}{a_0} \tag{9}$$

and is guaranteed to hold when the intra-cavity flat-lock solution is achieved because the steady-state magnitude $a_0 = |\psi_e|$ satisfies

$$a_0^2[1 + (\alpha - a_0^2)^2] = F_P^2 \tag{10}$$

and therefore, $F_P^2/a_0^2 = 1 + (\alpha - a_0^2)^2 > (\alpha - a_0^2)^2$; see Section II. For pump power F_P^2 chosen such that $a_0^2 \gg \alpha$, satisfying the synchronization condition becomes harder. This is where the system enters a chaotic state, as has been studied, for instance, in [27], [34]. Equation (8) can be integrated analytically and the final (steady-state) value of ϕ_0 is $2\tan^{-1}[(\sqrt{1-K^2}-1)/K]$, which, for the example shown in Fig. 3(c), equals 0.2718π and is within 3% of the value 0.26248π found from the numerical integration of the LLE of Eq. (1). We note that ϕ_P defines a phase reference and its specific value is immaterial.

5. Few-Mode Truncations of the LLE

5.1. Three-Mode Truncation

Equations of the temporal evolution of the centered phase averages $\zeta_\eta = \bar{\phi}_\eta - \phi_0$, where the phase average $\bar{\phi}_\eta = (\phi_\eta + \phi_{-\eta})/2$ is centered relative to the pumped mode phase ϕ_0, can be found from (6) and (7b). This equation, for the case of 3-wave truncation of the LLE ($\eta \in \{-\mu, 0, \mu\}$) reads

$$\frac{d}{d\tau}\zeta_\mu = \frac{1}{2}d_2\mu^2 + a_0^2[1 + \cos(2\zeta_\mu)] - \frac{F_P}{a_0}\sin(\phi_P - \phi_0) \tag{11}$$

and can be integrated analytically:

$$\tan\zeta_\mu = \sqrt{\left|\frac{C+2}{C}\right|}\tanh[\sqrt{|C(C+2)|}a_0^2(\tau - \tau_0)]. \tag{12}$$

In this equation, $C = d_2\mu^2/2a_0^2 - F_P\sin(\phi_P - \phi_0)/a_0^3$, and τ_0 accounts for the initial conditions. Equation (12) holds when $\rho_e > |2\rho_e - \alpha + d_2\mu^2/2|$, which is automatically satisfied when MI gain exists (see Section II). The tanh(·) function rapidly approaches unity as $\tau \to \infty$, and so, $\bar{\phi}_\mu$ reaches the same constant irrespective of the initial conditions. As $\bar{\phi}_\mu - \phi_0$ is fixed, the phases $\phi_{\pm\mu}$ should take values symmetrically located relative to the constant average and follow the changes in ϕ_0, as can be seen in Fig. 3(c). This constraint on the phases was noticed numerically by Wen *et al.* and termed "*phase anti-symmetrization*"; the expression given above simply justifies why phases anti-symmetrize. Therefore, the 3-mode truncation establishes that centered phase average ζ_μ can be treated as a constant to first order in $a_{\eta\neq 0}$. Note, however, that this approximation says nothing about the evolution of the phase differences (PDs) $\Delta_\mu = (\phi_\mu - \phi_{-\mu})/2$; the temporal evolution of the PDs simply follows $d\Delta_\mu/d\tau = 0$, stating that in the 3-mode truncation, a constant difference will rapidly be established between the sideband phases, as seen in Fig. 3(d). It is noteworthy that the assumed symmetry of the sideband powers (noted following (5)) indeed holds, as seen in Fig. 3(b).

5.2. Five-Mode Truncation

We now proceed one step further by including the second pair of sidebands, $\eta = \pm 2\mu$. Fig. 4 shows that the behavior of the pumped mode and primary sidebands magnitudes and phases does not change noticeably compared to the 3-mode truncation; this change is less than 2%. However, the PD equations for $\eta = \mu$ changes. The temporal evolution of the PDs take the form

$$\frac{d\Delta_\mu}{d\tau} = -2a_0a_{2\mu}\sin(\zeta_{2\mu} - 2\zeta_\mu)\sin(\Delta_{2\mu} - 2\Delta_\mu) \tag{13a}$$

$$\frac{d\Delta_{2\mu}}{d\tau} = -a_0\frac{a_\mu^2}{a_{2\mu}}[2\sin(\zeta_2) + \sin(\zeta_{2\mu} - 2\zeta_\mu)]\sin(\Delta_{2\mu} - 2\Delta_\mu). \tag{13b}$$

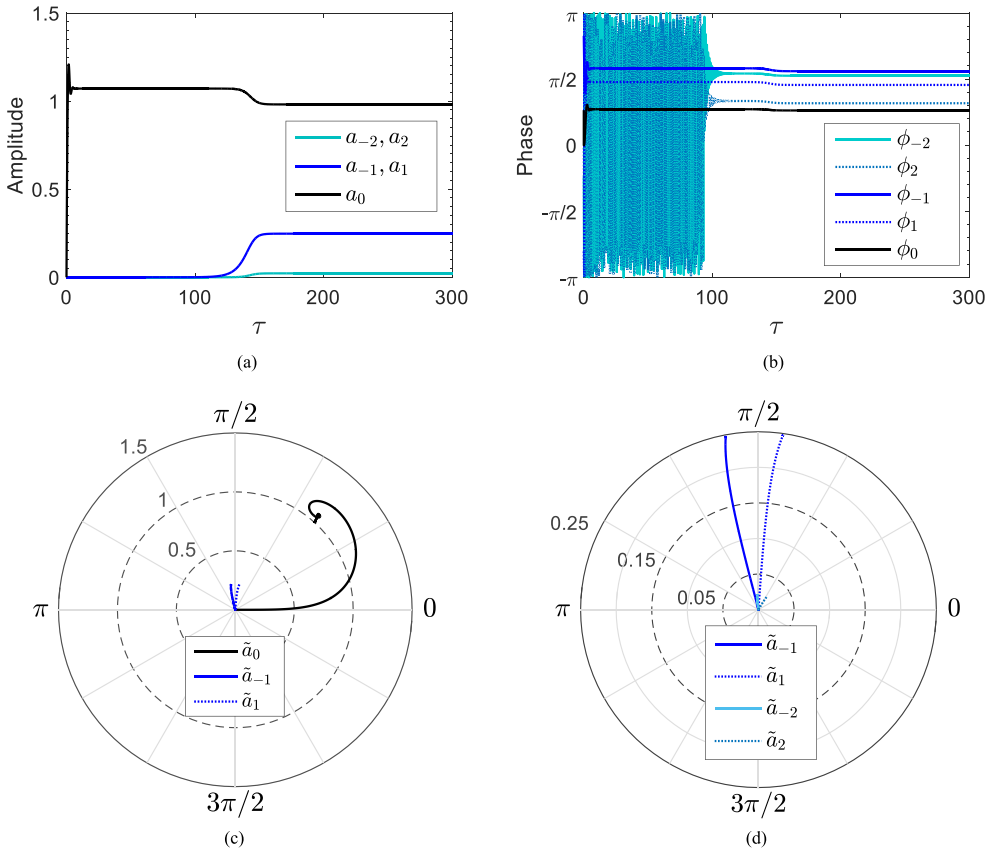

Fig. 4. Evolution of the pumped mode and sideband magnitudes and phases in the five-mode truncation of the LLE for comb parameters as in Fig. 1(d). (a) Pumped mode and sideband magnitudes. (b) Pumped mode and sideband phases. (c) Evolution of the comb teeth complex amplitudes in polar coordinates. (d) Zoomed-in version of (c) showing the complex amplitude of the first and second sidebands. While different initial conditions lead to different final phase values, the relationship $\phi_{2\mu} - \phi_{-2\mu} = 2(\phi_\mu - \phi_{-\mu})$ is always satisfied in the steady state. In the example shown here, $(\phi_{2\mu} - \phi_{-2\mu})/2 = \phi_\mu - \phi_{-\mu} = -0.104\pi$. ± 1 and ± 2 refer to the first and second sideband pairs labeled $\pm\mu$ and $\pm 2\mu$ in the text.

We note that these equations are written in the strong pumping regime to first order in $a_{\eta \neq 0}$, and can be combined to give a separable equation

$$\frac{\mathrm{d}}{\mathrm{d}\tau}(\Delta_{2\mu} - 2\Delta_\mu) = -a_0 f \sin(\Delta_{2\mu} - 2\Delta_\mu) \tag{14}$$

in which

$$f = 2\frac{a_\mu^2}{a_{2\mu}}\sin(\zeta_\mu) + \left(\frac{a_\mu^2}{a_{2\mu}} - 4a_{2\mu}\right)\sin(\zeta_{2\mu} - 2\zeta_\mu). \tag{15}$$

Equation (14) has analytical solution of the form

$$\tan[s(\tau)] = \tan[s(\tau_1)]\exp[-a_0 f(\tau - \tau_1)] \tag{16}$$

where $s(\tau) = [\Delta_{2\mu}(\tau) - 2\Delta_\mu(\tau)]/2$ (called the phase misalignment parameter, for reasons that will become clear shortly) and τ_1 is a constant of integration which can physically be thought of as marking the moment when second sideband powers $a_{\pm 2\mu}$ are above the noise level such that divisions by $a_{2\mu}$ in (13b) and (15) are mathematically valid. The integration leading to the above equation relies on the phase anti-symmetrization established in the 3-mode truncation, and shows that if $f > 0$, irrespective of the value of $\Delta_{2\mu} - 2\Delta_\mu$ at τ_1, the exponential decay will take $\Delta_{2\mu} - 2\Delta_\mu$

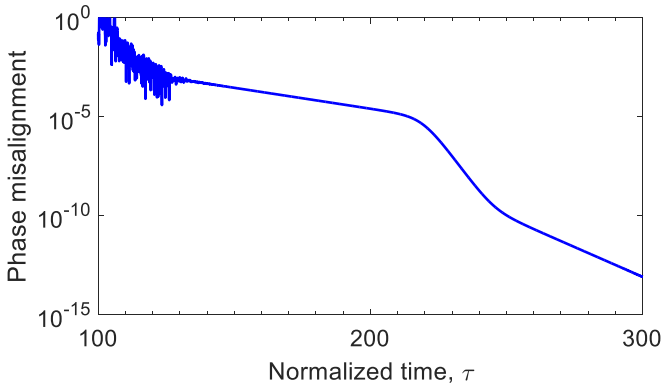

Fig. 5. Exponential decay of the phase misalignment parameter $s(\tau)$ with the normalized time τ in the full LLE, as predicted by (16). The early random oscillations are due to the small power in the sidebands early on in the generation of the comb, which leads to their phase wandering. The change in the slope of $s(\tau)$ reflects the growth of the sidebands as the comb evolves and is also captured by the few-mode models shown in Figs. 3 and 4. Note the dependence of the parameter f on the sideband powers in (15).

to zero. Physically, this amounts to the alignment of the phases of the first and second sideband pairs, because $\Delta_{2\mu}/2\mu = (\phi_{2\mu} - \phi_{-2\mu})/4\mu$ and $2\Delta_{\mu}/2\mu = (\phi_{\mu} - \phi_{-\mu})/2\mu$ are, respectively, slopes of the lines connecting $\phi_{2\mu}$ to $\phi_{-2\mu}$ and ϕ_{μ} to $\phi_{-\mu}$ in the phase vs. mode number plane. As a result, (16) predicts that the phase misalignment is dragged to zero upon phase locking. We show in Fig. 5 evolution of the misalignment parameter s as a function of the normalized time, found from the integration of the full LLE. This figure confirms that the requirement $f > 0$ is in fact met and the prediction of the exponential decay of $s(\tau)$ is correct (note the constant slopes and the logarithmic scale of the vertical axis). The changes in the slope at $\tau = 220$ and $\tau = 250$ occur because of the growth of the sideband powers as the comb evolves (recall the dependence of f on the sideband magnitudes in (15)). The reason these changes are shifted in time compared to those shown in Figs. 3 and 4 is that the power of seeding noise in our integration of the few-mode equations were not exactly matched with that in the split-step integration of the full LLE where noise power was smaller. The phase alignment described through the truncated equations and analytical expression in this section, justify the aligned phases of the Turing rolls shown in the lower panel of Fig. 2(d)–(f).

6. Summary and Outlook

In conclusion, based on few-mode truncations of the Lugiato-Lefever equation, we find analytical expressions which unfold the essence of the temporal evolution of comb teeth phases from random vacuum fluctuations toward locked steady states of sharply peaked pulses in the presence of modulational instability. We show that the pumped mode of the comb injection-locks to the driving pump laser frequency through the Adler equation. We also find, under assumptions motivated by experiments and using a three-mode truncation of the LLE, that sideband phases anti-symmetrize, i.e., their average becomes fixes with respect to the pumped mode phase before phase locking occurs. Considering the 5-mode truncation of the LLE, we derive an analytical expression describing how the phases of the comb teeth align irrespective of their initial values supplied by noise. This analysis shows that the phase misalignment of the comb sidebands dies exponentially with time until these phases all lie on a straight line. We confirm this prediction through numerical integration of the full LLE. The LLE is an externally-driven, damped nonlinear Schrödinger equation and has been used for describing a variety of physical phenomena in different nonlinear systems. The results presented here are mathematically generic and apply also to other systems beyond microcombs which are described by this variant of the NLSE. While the procedure for soliton formation is different from that of the generation of Turing rolls (i.e., hard vs. soft excitation [34], [47]), the nonlinear

coupling of the comb phases due to Kerr nonlinearity is a common element in both processes. The relationship between the results presented in this work and the phase locking mechanism in solitons has been studied elsewhere [48].

References

[1] T. J. Kippenberg, R. Holzwarth, and S. Diddams, "Microresonator-based optical frequency combs," *Science*, vol. 332, no. 6029, pp. 555–559, 2011.
[2] A. A. Savchenkov, A. B. Matsko, V. S. Ilchenko, I. Solomatine, D. Seidel, and L. Maleki, "Tunable optical frequency comb with a crystalline whispering gallery mode resonator," *Phys. Rev. Lett.*, vol. 101, no. 9, 2008, Art. no. 093902.
[3] K. Saha *et al.*, "Modelocking and femtosecond pulse generation in chip-based frequency combs," *Opt. Exp.*, vol. 21, no. 1, pp. 1335–1343, 2013.
[4] T. Herr *et al.*, "Temporal solitons in optical microresonators," *Nature Photon.*, vol. 8, no. 2, pp. 145–152, 2014.
[5] V. Brasch *et al.*, "Photonic chip-based optical frequency comb using soliton cherenkov radiation," *Science*, vol. 351, no. 6271, pp. 357–360, 2016.
[6] X. Yi, Q.-F. Yang, K. Y. Yang, M.-G. Suh, and K. Vahala, "Soliton frequency comb at microwave rates in a high-q silica microresonator," *Optica*, vol. 2, no. 12, pp. 1078–1085, 2015.
[7] J. Pfeifle *et al.*, "Coherent terabit communications with microresonator Kerr frequency combs," *Nature Photon.*, vol. 8, no. 5, pp. 375–380, 2014.
[8] J. Pfeifle *et al.*, "Optimally coherent Kerr combs generated with crystalline whispering gallery mode resonators for ultrahigh capacity fiber communications," *Phys. Rev. Lett.*, vol. 114, no. 9, 2015, Art. no. 093902.
[9] W. Liang *et al.*, "High spectral purity Kerr frequency comb radio frequency photonic oscillator," *Nature Commun.*, vol. 6, 2015, Art. no. 7957.
[10] I. Barashenkov and Y. S. Smirnov, "Existence and stability chart for the ac-driven, damped nonlinear Schrödinger solitons," *Phys. Rev. E*, vol. 54, no. 5, 1996, Art. no. 5707.
[11] A. Matsko, A. Savchenkov, W. Liang, V. Ilchenko, D. Seidel, and L. Maleki, "Mode-locked Kerr frequency combs," *Opt. Lett.*, vol. 36, no. 15, pp. 2845–2847, 2011.
[12] L. A. Lugiato and R. Lefever, "Spatial dissipative structures in passive optical systems," *Phys. Rev. Lett.*, vol. 58, no. 21, 1987, Art. no. 2209.
[13] M. Haelterman, S. Trillo, and S. Wabnitz, "Dissipative modulation instability in a nonlinear dispersive ring cavity," *Opt. Commun.*, vol. 91, no. 5, pp. 401–407, 1992.
[14] S. Coen, H. G. Randle, T. Sylvestre, and M. Erkintalo, "Modeling of octave-spanning Kerr frequency combs using a generalized mean-field Lugiato-Lefever model," *Opt. Lett.*, vol. 38, no. 1, pp. 37–39, 2013.
[15] Y. K. Chembo and C. R. Menyuk, "Spatiotemporal Lugiato-Lefever formalism for Kerr-comb generation in whispering-gallery-mode resonators," *Phys. Rev. A*, vol. 87, no. 5, 2013, Art. no. 053852.
[16] T. S. Raju, C. N. Kumar, and P. K. Panigrahi, "On exact solitary wave solutions of the nonlinear Schrödinger equation with a source," *J. Phys. A: Math. Gen.*, vol. 38, no. 16, 2005, Art. no. L271.
[17] W. H. Renninger and P. T. Rakich, "Closed-form solutions and scaling laws for Kerr frequency combs," *Sci. Rep.*, vol. 6, 2016, Art. no. 24742.
[18] P. DelHaye, K. Beha, S. B. Papp, and S. A. Diddams, "Self-injection locking and phase-locked states in microresonator-based optical frequency combs," *Phys. Rev. Lett.*, vol. 112, no. 4, 2014, Art. no. 043905.
[19] P. DelHaye, A. Coillet, W. Loh, K. Beha, S. B. Papp, and S. A. Diddams, "Phase steps and resonator detuning measurements in microresonator frequency combs," *Nature Commun.*, vol. 6, 2015, Art. no. 5668.
[20] A. B. Matsko, A. A. Savchenkov, D. Strekalov, V. S. Ilchenko, and L. Maleki, "Optical hyperparametric oscillations in a whispering-gallery-mode resonator: Threshold and phase diffusion," *Phys. Rev. A*, vol. 71, no. 3, 2005, Art. no. 033804.
[21] W. Loh, P. DelHaye, S. B. Papp, and S. A. Diddams, "Phase and coherence of optical microresonator frequency combs," *Phys. Rev. A*, vol. 89, no. 5, 2014, Art. no. 053810.
[22] A. Coillet and Y. Chembo, "On the robustness of phase locking in Kerr optical frequency combs," *Opt. Lett.*, vol. 39, no. 6, pp. 1529–1532, 2014.
[23] Y. H. Wen, M. R. Lamont, I. M. Kloumann, S. H. Strogatz, and A. L. Gaeta, "Self-organization in soliton modelocked parametric frequency combs," *arXiv:1412.0119*, 2014.
[24] S. H. Strogatz, "From Kuramoto to Crawford: Exploring the onset of synchronization in populations of coupled oscillators," *Physica D*, vol. 143, no. 1, pp. 1–20, 2000.
[25] I. V. Barashenkov and E. V. Zemlyanaya, "Travelling solitons in the externally driven nonlinear Schrödinger equation," *J. Phys. A: Math. Theor.*, vol. 44, no. 46, 2011, Art. no. 465211.
[26] M. R. Lamont, Y. Okawachi, and A. L. Gaeta, "Route to stabilized ultrabroadband microresonator-based frequency combs," *Opt. Lett.*, vol. 38, no. 18, pp. 3478–3481, 2013.
[27] A. Coillet and Y. K. Chembo, "Routes to spatiotemporal chaos in Kerr optical frequency combs," *Chaos: Interdisciplinary J. Nonlinear Sci.*, vol. 24, no. 1, 2014, Art. no. 013113.
[28] P. DelHaye, A. Schliesser, O. Arcizet, T. Wilken, R. Holzwarth, and T. Kippenberg, "Optical frequency comb generation from a monolithic microresonator," *Nature*, vol. 450, no. 7173, pp. 1214–1217, 2007.
[29] J. K. Jang, M. Erkintalo, S. G. Murdoch, and S. Coen, "Writing and erasing of temporal cavity solitons by direct phase modulation of the cavity driving field," *Opt. Lett.*, vol. 40, no. 20, pp. 4755–4758, 2015.
[30] H. Taheri, A. Eftekhar, K. Wiesenfeld, and A. Adibi, "Soliton formation in whispering-gallery-mode resonators via input phase modulation," *IEEE Photon. J.*, vol. 7, no. 2, Apr. 2015, Art. no. 2200309.
[31] P. Grelu and N. Akhmediev, "Dissipative solitons for mode-locked lasers," *Nature Photon.*, vol. 6, no. 2, pp. 84–92, 2012.

[32] Y. K. Chembo and N. Yu, "Modal expansion approach to optical-frequency-comb generation with monolithic whispering-gallery-mode resonators," *Phys. Rev. A*, vol. 82, no. 3, 2010, Art. no. 033801.
[33] T. Herr *et al.*, "Universal formation dynamics and noise of Kerr-frequency combs in microresonators," *Nature Photon.*, vol. 6, no. 7, pp. 480–487, 2012.
[34] C. Godey, I. V. Balakireva, A. Coillet, and Y. K. Chembo, "Stability analysis of the spatiotemporal Lugiato-Lefever model for Kerr optical frequency combs in the anomalous and normal dispersion regimes," *Phys. Rev. A*, vol. 89, no. 6, 2014, Art. no. 063814.
[35] G. Kozyreff, "Localized turing patterns in nonlinear optical cavities," *Phys. D: Nonlinear Phenomena*, vol. 241, no. 10, pp. 939–946, 2012.
[36] H. Taheri, A. B. Matsko, and L. Maleki, "Optical lattice trap for Kerr solitons," *arXiv preprint arXiv: 1704.00024*, 2017.
[37] A. V. Oppenheim and R. W. Schafer, *Discrete-Time Signal Processing*. Upper Saddle River, NJ, USA: Prentice-Hall, 1989.
[38] G. P. Agrawal, *Nonlinear Fiber Optics*, 5th ed. San Diego, CA, USA: Academic, 2013.
[39] Y. K. Chembo, D. V. Strekalov, and N. Yu, "Spectrum and dynamics of optical frequency combs generated with monolithic whispering gallery mode resonators," *Phys. Rev. Lett.*, vol. 104, no. 10, 2010, Art. no. 103902.
[40] S.-W. Huang *et al.*, "Mode-locked ultrashort pulse generation from on-chip normal dispersion microresonators," *Phys. Rev. Lett.*, vol. 114, no. 5, 2015, Art. no. 053901.
[41] S. Trillo and S. Wabnitz, "Dynamics of the nonlinear modulational instability in optical fibers," *Opt. Lett.*, vol. 16, no. 13, pp. 986–988, 1991.
[42] S. Trillo, S. Wabnitz, and T. Kennedy, "Nonlinear dynamics of dual-frequency-pumped multiwave mixing in optical fibers," *Phys. Rev. A*, vol. 50, no. 2, 1994, Art. no. 1732.
[43] A. A. Savchenkov, A. B. Matsko, D. Strekalov, M. Mohageg, V. S. Ilchenko, and L. Maleki, "Low threshold optical oscillations in a whispering gallery mode CaF2 resonator," *Phys. Rev. Lett.*, vol. 93, no. 24, 2004, Art. no. 243905.
[44] T. Hansson, D. Modotto, and S. Wabnitz, "Dynamics of the modulational instability in microresonator frequency combs," *Phys. Rev. A*, vol. 88, no. 2, 2013, Art. no. 023819.
[45] H. Taheri, A. A. Eftekhar, K. Wiesenfeld, and A. Adibi, "Anatomy of phase locking in parametric frequency combs," *Proc. Frontiers Opt.*, 2015, Paper JW2A.12. [Online]. Available: http://www.osapublishing.org/abstract.cfm?URI=FiO-2015-JW2A.12
[46] R. Adler, "A study of locking phenomena in oscillators," *Proc. IRE*, vol. 34, no. 6, pp. 351–357, Jun. 1946.
[47] A. B. Matsko, A. A. Savchenkov, V. S. Ilchenko, D. Seidel, and L. Maleki, "Hard and soft excitation regimes of Kerr frequency combs," *Phys. Rev. A*, vol. 85, no. 2, 2012, Art. no. 023830.
[48] H. Taheri, P. Del'Haye, A. A. Eftekhar, W. Kurt, and A. Ali, "Self-synchronization phenomena in the Lugiato-Lefever equation," 2016, submitted for publication.